ELSEVIER

Thermochimica Acta 357–358 (2000) 259–266

thermochimica acta

www.elsevier.com/locate/tca

Thermal analysis of paraffins by calorimetry☆

J. Pak[a,b], A. Boller[a,b], I. Moon[a,b], M. Pyda[a,b], B. Wunderlich[a,b,*]

[a]*Department of Chemistry, The University of Tennessee, Knoxville, TN 37996-1600, USA*
[b]*Chemical and Analytical Sciences Division, Oak Ridge National Lab., Oak Ridge, TN 37831-6197, USA*

Received 9 November 1998; accepted 17 January 1999

Abstract

Paraffins of sufficient chain length can serve as model compounds for flexible macromolecules. They crystallize almost completely and do not suffer from chain folding as long as their chain length is less than about 10 nm. The melting and crystallization of a paraffin, $C_{50}H_{102}$ (*n*-pentacontane), was analyzed as such a model compound with both, standard differential scanning calorimetry (DSC) and temperature-modulated DSC (TMDSC) using saw-tooth modulation and quasi-isothermal modulation with very small amplitude (0.05 K). The supercooling due to nucleation was shown to be strongly cooling-rate dependent. There was practically no supercooling needed for crystallization from the melt with cooling rates up to 10 K/min, and values of up to 10 K were found for cooling rates of 30 K/min. Melting was completed within 1 K with quasi-isothermal modulation, but 66% of total melting occurred over a much narrower temperature range of 0.1 K or less. A 'reversing' melting in the paraffin was detected by TMDSC and the previously proposed integral analysis is found to be a useful tool for quantitative analysis of the thermal transition. Published by Elsevier Science B.V.

Keywords: Thermal analysis; Paraffin; Phase transition; $C_{50}H_{102}$; Equilibrium; Non-equilibrium

1. Introduction

Temperature-modulated differential scanning calorimetry (TMDSC), in the melting and crystallization region of linear macromolecules is complicated by the need to evaluate the reversible heat capacity in the presence of superimposed, latent-heat effects which are often non-reversing. The latent heat may be absorbed or evolved abruptly, causing difficulties in the Fourier analysis of the apparent heat capacity, so that the data treatment has to be carried out on the raw heat-flow and sample-temperature data in the time domain (HF(t) and $T_s(t)$, respectively) [1]. Despite these difficulties, TMDSC offers the possibility of new insight into the microstructure of polymers by yielding information on re-crystallization, crystal perfection, melting and crystallization kinetics, and metastability. First experiments over the last two years have resulted in the observation of the expected full irreversibility of melting of polymers [2,3], but also the kinetics of small amounts of partially or fully-reversible, local, latent-heat effects [2–5]. To quantify these observations, experiments were carried out on the fully reversible sharp melting and (nucleated) crystallization of indium [6], and the low latent-heat, but sharp and also reversible isotropization and ordering of liquid crys-

* Corresponding author.

0040-6031/00/$ – see front matter Published by Elsevier Science B.V.
PII: S0040-6031(00)00396-8

tals [7]. Also, the independence of the observed phenomena from the type of instrumentation was documented [8]. In this paper, the behavior of the small, but flexible molecule *n*-pentacontane, $C_{50}H_{102}$, will be described as a model compound for linear macromolecules.

2. Experimental

A Mettler–Toledo DSC 820 was used for all measurements, except for the quasi-isothermal analyses [9,10] which were done with the Thermal Analyst 2920 system from TA Instruments. Fig. 1 shows a schematic of the dynamic DSC, DDSC^{TM} of Mettler–Toledo. Dry N_2 gas with a flow rate of 20 ml/min was purged through the DSC cell in both the instruments. Cooling was accomplished with a liquid-nitrogen cooling-accessory or a refrigerated cooling system (RCS, cooling capacity to 220 K). The temperature of the equipment was initially calibrated in the standard DSC mode using the onset of the transition peaks for indium (429.75 K), naphthalene (353.42 K), *n*-octane (116.4 K), acetone (177.9 K), cyclohexane (s/s 186.09 and s/l 297.7 K), cycloheptane (265.1 K), and Sn (505.05 K) at a scanning rate of 10 K/min. The heat-flow rate was calibrated with the heat of fusion of indium (28.45 J/g). The onset of

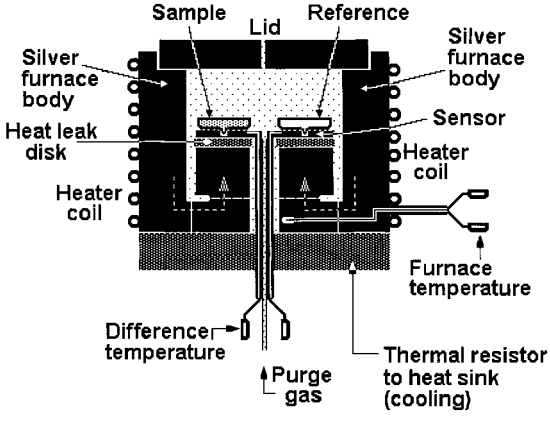

Fig. 1. Schematic drawing of the Mettler–Toledo DDSCTM furnace. The calorimeter is modulated at the furnace temperature. The sensor consists of multiple thermocouples, to give an averaged, sensitive measurement of the temperature difference, ΔT. The true reference temperature is obtained by calibration. Drawn after Mettler–Toledo instrument descriptions.

melting was determined by extrapolating the sample temperature from the linear portion of the melting peak to the baseline [11].

The sample masses for the standard DSC were 1.894 and 0.580 mg for saw-tooth modulation, and 0.936 mg for quasi-isothermal measurements with sinusoidal modulation. The samples were weighed on a Cahn C-33 electro-balance to an accuracy of ±0.001% of the total load (50 mg). For the Mettler–Toledo DSC 820, the samples were encapsulated in the 40-μl standard aluminum crucibles without center pins and with a cold-welded cover. The reference pan was an aluminum crucible with a center pin and a cover for the standard DSC experiments and an Al-crucible with a center pin and without a cover for the TMDSC measurements. The TA Instruments MDSC 2929 was used with standard Al pans with covers for the samples and as empty reference.

The onset temperatures of the transitions of *n*-pentacontane were measured in the standard DSC-mode as a function of the scanning rate (from ±1 to ±30 K/min). Heating at 7.24 K/min and cooling at 5.24 K/min were carried out for the saw-tooth modulation, which leads to an underlying heating rate of $\langle q \rangle$ of 1.0 K/min and a modulation period, p=90 s. Quasi-isothermal TMDSC ($\langle q \rangle$=0) was done with a very small modulation amplitude of A=0.05 K, a sinusoidal modulation period of p=60 s, and step-wise temperature-increments of 0.1 K (=ΔT_0) between successive data sets. Each quasi-isothermal measurement lasted 40 min. The last 10 min were used for data collection needed for the evaluation of the heat capacity.

The paraffin discussed in this paper is *n*-pentacontane ($C_{50}H_{102}$), obtained from Aldrich, Milwaukee, WI. Its purity is 99+%. Data bank values for the equilibrium melting temperature, T_m, and the heat of fusion at T_m, H_f, are 365.30 K, and 224.87 J/g, respectively [12]. Most precise melting temperatures of the *n*-pentacontane were determined with a Mettler hot stage FP-82 mounted on an Olympus stereo-microscope, calibrated at the melting temperature of indium. The temperature of the disappearance of birefringence at a magnification of about 50× was taken as the melting temperature on repeated melting and crystallization of about 550 μm big crystals at a heating rate of 0.1 K/min. The melting temperature under these conditions is 365.3±0.05 K.

3. Results and discussion

3.1. Standard DSC measurement

Fig. 2 shows the onset-temperatures of melting and crystallization for the paraffin as a function of the scanning rate. The onset-temperatures change little for the scanning rates from −10 to +10 K/min. The equation in the figure and the drawn line give the average change for a scanning rate above −10 K/min. This result indicates that the standard DSC of $C_{50}H_{102}$ shows almost no supercooling for the normally used scanning rates of ±10 K/min and suggests that *n*-pentacontane disorders less on melting and undergoes faster nucleation than observed for linear macromolecules. The latter needs molecular nucleation for crystallization in addition to crystal nucleation, causing considerable supercooling even on slow cooling [13].

Below the cooling rate of 10 K/min the onset of crystallization changes drastically. This behavior is different from the melting and crystallization of indium which supercools by about 1.0 K at all cooling rates [6]. The results of some 25 additional experiments on $C_{50}H_{102}$ done to elucidate this behavior were not entirely quantitative so that further experimentation is needed. The onset of supercooling that occurs in Fig. 2 at −10 K/min could be moved beyond −20 K/min by immediate cooling after melting. Holding the sample for as long as 100 min at 400 K followed by cooling at 10 K/min or slower never gave supercooling.[1]

3.2. Saw-tooth modulation and integral analysis

Fig. 3 illustrates the results of the melting and crystallization generated by TMDSC measurement with a saw-tooth modulation and an underlying heating rate of 1.0 K/min. The dashed curve represents the time-dependent heat-flow rate, HF(*t*). It increases strongly in the melting and crystallization regions of the *n*-pentacontane. The solid curve represents the sample temperature. In the melting and crystallization regions, it deviates from the expected saw-tooth temperature-program (dotted) because of the absorption and evolution of the latent heat. Odd numbered peaks mark the melting and even numbers, the crystallization. The heats of transition, ΔH, taken over an appropriate baseline, are summarized in Table 1. Peaks 3, 4, 5 agree within experimental error with the heat of transition of $C_{50}H_{102}$ known to be 224.78 J/g [12]. The onsets of melting from peaks 1, 3, and 5, are ca. 0.25 K higher than the onsets of crystallization from peaks 4 and 6. This difference is in reasonable agreement with the expected shift of these

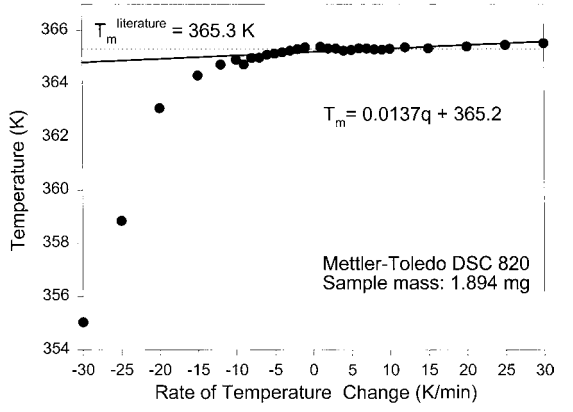

Fig. 2. Onset temperature of transition of *n*-pentacontane as a function of scanning rate as measure by standard DSC.

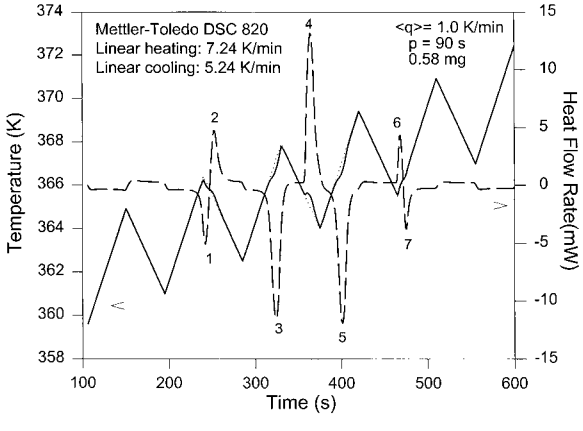

Fig. 3. Modulated heat-flow rate and sample temperature, plotted vs. time for a saw-tooth modulation TMDSC run. The dashed curve is the modulated heat-flow rate. The solid line represents the sample temperature. The dotted line denotes the saw-tooth temperature program. Odd numbers are for melting and even numbers for crystallization peaks.

[1] Since the same samples analyzed in other calorimeters do not show the same supercooling. This observation is most likely caused by the instrument.

Table 1
Heats of fusion by integral analysis from TMDSC, of the run shown in Fig. 3

Number[a]	ΔH (J/g)	$\Delta H/\Delta H_0$[b] (%)	Height ratio (%)
1	63.59	28.290	29.2
2	−69.41	−30.879	29.2
3	215.84	96.023	97.7
4	−217.24	−96.646	97.7
5	220.32	98.016	98.5
6	−29.77	−13.244	15.2
7	34.30	15.259	15.2

[a] The numbers correspond to the peak numbers in Fig. 3.
[b] ΔH_0 is the total heat of fusion of $C_{50}H_{102}$.

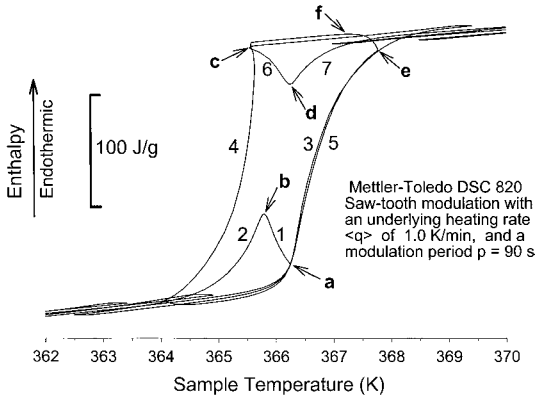

Fig. 5. Enthalpy as given by the integral analysis of Fig. 3 as a function of reference temperature.

onsets with heating and cooling rates as given in Fig. 2 (0.17 K). Using an integral analysis, as described in Ref. [14], one can get clear information about the degree of completion of the transition during each cycle. Such analysis is shown in Fig. 4. The solid curve was obtained by integrating the heat-flow curve of Fig. 3. The dotted curves are extrapolations from the integral data before, and after, the transition region. The dotted curve at the bottom represents the enthalpy of the crystalline paraffin, and, at the top, the enthalpy of the liquid paraffin. Each height of the deviation from the dotted curve corresponds to the heat of transition exchanged during each peak in Fig. 3. These values are also summarized in Table 1. Just measuring the height of the enthalpy gives an answer of how much of the crystal melts and

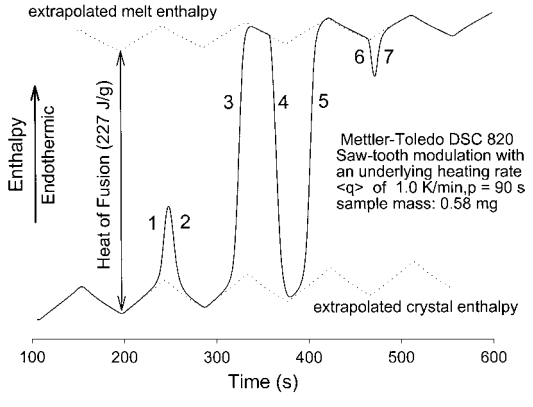

Fig. 4. Enthalpy as given by the integral analysis in the time domain for the saw-tooth TMDSC run of Fig. 3.

how much melt crystallizes in each segment of the saw-tooth. Fig. 5 represents a transposition of Fig. 4 to a plot vs. sample temperature. It permits an interpretation of the behavior of the sample during each of the transition peaks. The heat-flow rate HF(t) is proportional to the temperature difference between the temperatures of the reference and sample sensors, $\Delta T = T_r - T_s$.

In the first, incomplete melting, represented by peak 1 in Fig. 3, the heating cycle switches to cooling at the point 'a' of Fig. 5. Since the modulation is controlled at the furnace (see Fig. 1), one notes at this point hardly any change in the rate of melting (see Fig. 4). In the interior of the sample, melting continues up to point 'b'. At this point, which is close to the onset of melting, the excess melting stops and one reaches a dynamic melting/crystallization equilibrium (compare Figs. 4 and 5). This is followed by excess crystallization, visible as peak 2 in Fig. 3. One can deduce from Fig. 4 that the total amount of melting during peak 1 is about 30%, all of which crystallizes again during the cooling cycle (see Table 1). Fig. 3 indicates, furthermore, that at point 'b' the sample temperature equals the program temperature. One estimates, thus, from the temperature difference between the two points 'a' and 'b' in Fig. 5 a temperature gradient of about 0.5 K between the melt interface of the crystals in the interior of the sample pan and at the bottom of the pan. Similarly, the partial crystallization and melting peaks 6 and 7 set up a temperature gradient of about 0.7 K in the sample pan at point 'd', at which point about 15% of the sample has

crystallized. The difference between temperatures 'b' and 'd' is 0.4 K, or 0.2 K after the extrapolation with help of Fig. 2 to rate zero of temperature change. As will be shown in the discussion of peak 4, this slightly higher temperature of 'd' than of 'b' may well be caused by the self-heating during the crystallization exotherm.

Melting peak 3 also continues into the cooling cycle, as shown by points 'e' and 'f'. Point 'f' is, however, above the melting temperature. The next crystallization does not commence until peak 4 is reached. The time between peaks 3 and 4 is sufficient to establish steady-state cooling of the melt (see Fig. 3). Table 1 indicates that, despite the temperature reversal before completion of melting, melting was practically complete.

Complete crystallization on cooling, followed by melting on heating, with near attainment of an intermediate steady state are given by peaks 4 and 5, respectively. The two peaks show the typical asymmetry of crystallization and melting. The total temperature lag from the onset of melting to regaining of steady state in Fig. 5 is almost 3 K under the given experimental conditions. On crystallization, latent heat is produced and actually raises the sensor temperature of the sample, as documented by the positive deviation of the cooling segment 4 in Fig. 5. With a sufficient amount of crystallization and high thermal conductivity, the temperature of the sample sensor would have reached the melting temperature sensor, as was observed for the TMDSC of indium [14]. The total temperature lag from the onset of crystallization to regaining of steady state is only 1.5 K under the given experimental conditions.

This observation of the temperature profiles during melting and crystallization leads to the following picture: On heating, the temperature of the remaining unmelted crystals is constant at the equilibrium melting temperature. This lack of superheating of crystals is common, since the melting rates of most materials are faster than the delivery of the needed heat of fusion through heat conduction [11,13]. The constant temperature of the remaining crystals generates a colder core within the sample pan with a crystal/melt interface of the equilibrium melting temperature. Direct temperature measurement during heating of the sample pan with a cover has shown that the pan and the cover have practically the same temperature [15], so that the unmelted portion of the sample is expected to be located in the middle of the pan if there is a cover, and close to the upper surface when the pan has no cover. Outside of the crystal/melt interface, the melt gets hotter as one approaches the walls of the pan. On cooling, crystallization is first expected in the vicinity of the walls of the pan if no or only little supercooling is needed, as in the present case of *n*-pentacontane. If supercooling occurs, one can produce a case where the unmelted core of crystals increases and decreases in response to cooling and heating, without additional crystal growth away from the core of crystals. This situation was probably reached in the case of TMDSC of indium [14]. In the case of indium, the exotherm on crystallization of the melt with supercooling was, in addition, sufficient to heat the growing crystals and their surrounding melt to the equilibrium melting temperature [14]. One may find, thus, two different volumes in the sample pan on TMDSC. One is represented by the crystals at the melting temperature, the other by the surrounding melt which increases or decreases in temperature at a rate balanced by the heat-flow rate. On heating with partial melting, followed by cooling with crystallization without supercooling, as for $C_{50}H_{102}$, crystals at the melting temperature may be found not only in the center of the pan, but also at the bottom, separated by a volume of some melt at a higher temperature. Each of the different scenarios needs a separate model for quantitative interpretation which has not been attempted as yet. Also, the picture will be complicated if the crystal density is sufficiently large to make the remaining crystals sink to the bottom and disturb the temperature gradient.

3.3. Quasi-isothermal modulation

In view of the large lags observed in TMDSC with an underlying heating rate, quasi-isothermal experiments with sinusoidal modulation were carried out to identify the intrinsic melting behavior of $C_{50}H_{102}$. This type of TMDSC avoids much of the instrument lag. The quasi-isothermal TMDSC experiments were carried out with the very small modulation amplitude of 0.05 K and were repeated in three separate experiments under the same conditions to assure reproducible results. Because of the high precision in

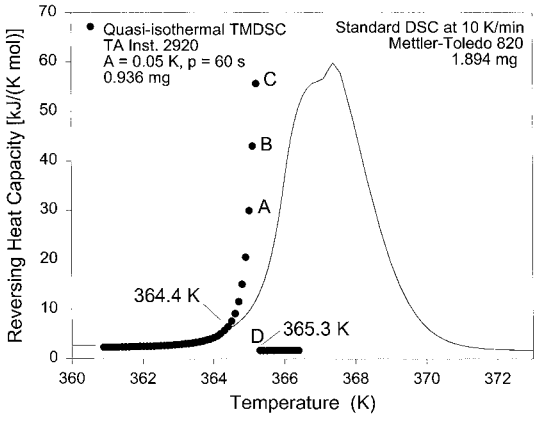

Fig. 6. Reversing heat capacity of *n*-pentacontane by standard DSC and quasi-isothermal TMDSC. For the standard DSC, $\langle q \rangle$=10 K/min (solid curve). For quasi-isothermal TMDSC, A=0.05 K, p=60 s, $\langle q \rangle$=0, stepwise temperature-increments of 0.1 K (filled circles).

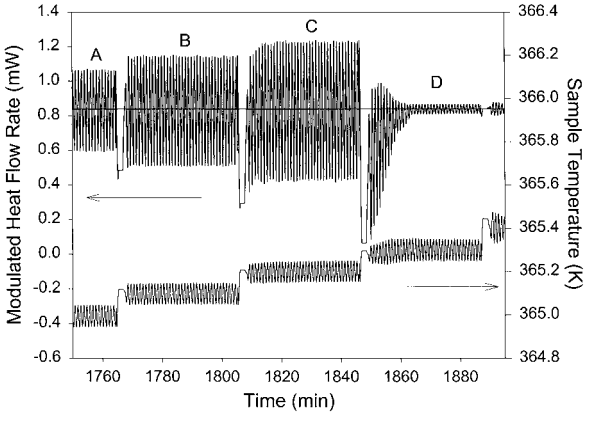

Fig. 7. Modulated heat-flow rate and sample temperature plotted vs. time for 0.936 mg *n*-pentacontane by quasi-isothermal TMDSC as in Fig. 6. In the downward direction HF(t) is endothermic.

temperature needed for the discussion of the quasi-isothermal experiments, all measurements with different calorimeters were calibrated with the melting point observed on the same *n*-pentacontane by optical microscopy. A series of typical quasi-isothermal runs are depicted in Fig. 6. Plotted is the reversing heat capacity, calibrated to yield the proper heat capacities in the crystal- and melt-region [16]. The method of quasi-isothermal measurement of the reversing heat capacity which represents the absolute magnitude of the complex heat capacity is described in the references listed in [9,10]. Fig. 6 shows that a small amount of reversible melting starts at 364.4 K with a first deviation from the crystal heat capacity as low as 362 K and ends at point D at a temperature of 365.30±0.05 K. The latter temperature is the first point that reproduces the value of the reversing heat capacity of the melt and is calibrated to agree with the disappearance of the birefringence in optical microscopy. A more detailed discussion of point D is given below.

The sum of all endotherms and exotherms generated during all quasi-isothermal runs of a set that cover the full melting range, including the endotherms generated for each heating step between successive quasi-isothermal runs, yields 221 J/g. This value is within the error limit equal to the total heat of fusion (224.78 J/g). The sum of the endotherms and exotherms for the quasi-isothermal experiment at 365.30±0.05 K alone (point D) is 137.4 J/g. This proves that the paraffin melts almost completely within 1.0 K, but 66% of the total melting occurs over the much narrower temperature range of 0.1 K from 365.25 to 365.35 K.

More information about the melting process can be gained from the modulated heat-flow rate HF(t) shown in Fig. 7. Up to the point C, the amplitudes of the heat-flow rates are symmetrical and quickly reach a steady state. Most of the 34% of heat of fusion absorbed before point D comes from the heating steps needed to achieve the temperature-increments between the runs. This means that up to, and including, measurement C, melting and crystallization are reversible in each modulation cycle. At point C, the crystallization and melting accounts for about 4% of the total crystallinity in each cycle.

On reaching point D, this reversible melting and crystallization and quick attainment of steady state is lost. More melting occurs in the first few cycles than crystallization. Finally, after 13 cycles, the sample settles into the reversing heat-flow rate characteristic for the liquid. Also, the modulation of the sample temperature of the initial part of run D does not follow the modulation program, i.e. T_s does not reach its programmed maxima, but overshoots the programmed minima for the first nine modulation cycles. The large amount of heat of transition could not be compensated properly by the modulation program which is

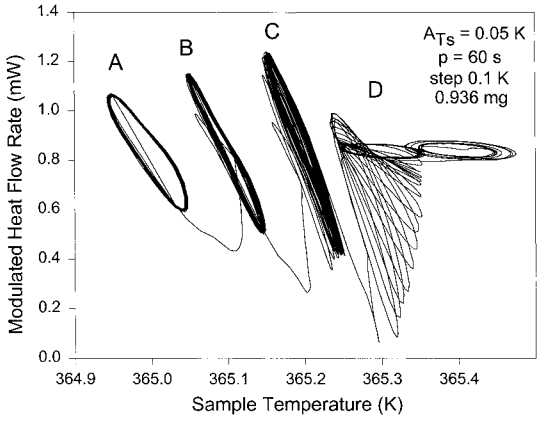

Fig. 8. Lissajous figures for the five quasi-isothermal TMDSC runs also shown in Fig. 6. In the downward direction HF(t) is endothermic.

governed for the TMDSC of TA Instruments by the sample-temperature sensor. This observation implies that the melting of the remaining 66% of the crystals should have been completed before the maximum temperature of the modulation of run D had been reached for the first time. One can conclude from this slow, asymmetric approach to the steady state for the liquid that the true melting end must be close to the minimum of the temperature modulation, 365.25 K. If T_m were above the midpoint of modulation, 365.30 K, one would again expect a symmetric steady state with a larger reversing heat capacity than found for the liquid.

Fig. 8 shows Lissajous figures for some of the same quasi-isothermal runs as shown in Figs. 6 and 7. A Lissajous figure is a plot of the modulated heat-flow rate vs. the modulated temperature and has been suggested as a means to analyze TMDSC traces [9,17]. Only the Lissajous figures for the liquid state and the (not shown) solid before melting are truly elliptical which is indicative of reversibility and (close to) constant heat capacity over the full range of modulation [18]. The Lissajous figures, A, B, and C, reach a steady state, but the apparent heat capacity changes with sample temperature. The Lissajous figure D reveals larger melting than crystallization and a continuous decrease in the transition activity as seen in Fig. 7.

Combining all information of Figs. 7 and 8, we conclude that the end of melting must be at 365.25±0.01 K. Crystallization cannot occur above the melting temperature. From Fig. 7, one can see that only the first nine cycles of run D reached below the minimum programmed temperature, i.e. they reached lower than the maximum of the modulation of run C which is still symmetric in crystallization and melting. Only these nine cycles show crystallization effects. From this observation, we conclude that the end of melting occurs within experimental error between the extremes of modulations for runs C and D, namely 365.25 K. The error to be assigned to this temperature must take account of the fact that no supercooling of the melt was observed, and that the steady state of run C is symmetric. Neither of these observations allows a variation of the melt end by more than 0.01 K.

4. Conclusions

The earlier analyses of well-crystallized poly(oxyethylene)s (POE) of 1500 and 5000 Da molar mass showed that melting of polymers is practically completely irreversible [2–5]. The major melting range of the polymers can be judged to be 2–3 K wide. This range was several times the modulation amplitude for these analyses (±0.5 K), i.e. in the melting range, crystal nuclei remain during the cooling cycle of quasi-isothermal modulation, but do not initiate recrystallization of any of the melted molecules [2,3]. The quasi-isothermal analysis of the melting of POE is, thus, taken as proof that molecular nucleation is needed in addition to crystal nucleation [4,5]. In contrast to the melting of polymers, indium shows reversible melting and crystallization as long as the melting during the heating cycle is incomplete and nuclei are left for re-crystallization during the cooling cycle [1,6]. In this case, there is no supercooling. Once, however, melting is complete; i.e. no nuclei are left, there is a supercooling of 1–1.5 K between indium melting and crystallization [6].

In comparison to indium and POE, *n*-pentacontane should be a molecule with an intermediate melting/crystallization behavior. The paraffin used in this research has a molar mass of 703 Da. Its chain length is about 6.2 nm, which is less than that of a typical

polymer-crystal thickness (≈10 nm) [13], excluding the possibility of chain folding of the paraffin on crystallization. Still, $C_{50}H_{102}$ has 47 bonds to produce as many as 2.7×10^{22} conformational isomers. It is possible to conclude from the fact the *n*-pentacontane needs increasing supercooling on fast cooling, particularly after longer holding of the melt above T_m, that the temperature-modulated DSC can be used as a tool to study the kinetics of changes of the rotational isomers. In DSC experiments with slow cooling rates $C_{50}H_{102}$ behaves like a small molecule and is not a model compound for polymers. On faster cooling, this changes and may permit a first insight into the kinetics of ordering of flexible chains.

It is also shown that quasi-isothermal TMDSC with very small amplitudes can give more precise data on reversibility in the presence of large heats of transition. The integral analysis has proven for such analysis to be a useful tool for the quantitative analysis of the transition.

Acknowledgements

This work was supported by the Division of Materials Research, National Science Foundation, Polymers Program, Grant # DMR-9703692 and the Division of Materials Sciences, Office of Basic Energy Sciences, US Department of Energy at Oak Ridge National Laboratory, managed by Lockheed Martin Energy Research Corporation for the US Department of Energy, under contract number DE-ACOS-960R22464.

References

[1] B. Wunderlich, I. Okazaki, K. Ishikiriyama, A. Boller, Thermochim. Acta 324 (1998) 77; see also: R.G. Morgan (Ed.), Proceedings 25th NATAS Conference in McLean, VA, 7–9 September, 1997, p. 49.
[2] K. Ishikiriyama, B. Wunderlich, Macromolecules 30 (1997) 4126.
[3] K. Ishikiriyama, B. Wunderlich, J. Polym. Sci., Part B: Polym. Phys. 35 (1997) 1877.
[4] I. Okazaki, B. Wunderlich, Macromol. Chem. Phys. Rapid Commu. 18 (1997) 313.
[5] I. Okazaki, B. Wunderlich, Macromolecules 30 (1997) 1758.
[6] K. Ishikiriyama, A. Boller, B. Wunderlich, J. Therm. Analy. 50 (1997) 547.
[7] W. Chen, B. Wunderlich, Thermochim. Acta 324 (1998) 87; see also: R.G. Morgan (Ed.), Proceedings 25th NATAS Conference in McLean, VA, 7–9 September, 1997, p. 637.
[8] C. Schick, M. Merzlyakov, B. Wunderlich, Polym. Bull. 40 (1997) 297.
[9] A. Boller, Y. Jin, B. Wunderlich, J. Therm. Analy. 42 (1994) 307.
[10] B. Wunderlich, Y. Jin, A. Boller, Thermochim. Acta 238 (1994) 277.
[11] B. Wunderlich, in: E. Turi (Ed.), Thermal Characterization of Polymeric Materials. Academic Press, San Diego, 1997; see also Thermal Analysis, Academic Press, Boston, 1990.
[12] B. Wunderlich, Pure Appl. Chem. 67 (1995) 1919; for data see the World Wide Web-site: http://web.utk.edu/~athas.
[13] B. Wunderlich, Macromolecular Physics, vol. II, Crystal Nucleation, Growth, Annealing, Academic Press, New York, 1976, and vol. III, Crystal Melting. Academic Press, New York, 1980.
[14] A. Boller, M. Ribeiro, B. Wunderlich, J. Therm. Analy. 54 (1998) 545.
[15] R. Androsch (unpublished observation by infrared thermometry).
[16] Y. Jin, B. Wunderlich, J. Phys. Chem. 95 (1991) 9000.
[17] M. Varma-Nair, B. Wunderlich, J. Therm. Analy. 46 (1996) 879.
[18] M. Pyda, B. Wunderlich, in: K.R. Williams (Ed.), Proceedings 26th NATAS Conference in Cleveland, OH, 13–15 September, 1998, 26 (1998) 287.